LUND UNIVERSITY

Intensity dependence of laser-assisted attosecond photoionization spectra

Swoboda, Marko; Dahlström, Marcus; Ruchon, Thierry; Johnsson, Per; Mauritsson, Johan; L'Huillier, Anne; Schafer, K. J.

Published in:
Laser Physics

DOI:
10.1134/S1054660X09150390

2009

Link to publication

Citation for published version (APA):
Swoboda, M., Dahlström, M., Ruchon, T., Johnsson, P., Mauritsson, J., L'Huillier, A., & Schafer, K. J. (2009). Intensity dependence of laser-assisted attosecond photoionization spectra. *Laser Physics*, *19*(8), 1591-1599. https://doi.org/10.1134/S1054660X09150390

Total number of authors:
7

General rights
Unless other specific re-use rights are stated the following general rights apply:
Copyright and moral rights for the publications made accessible in the public portal are retained by the authors and/or other copyright owners and it is a condition of accessing publications that users recognise and abide by the legal requirements associated with these rights.
• Users may download and print one copy of any publication from the public portal for the purpose of private study or research.
• You may not further distribute the material or use it for any profit-making activity or commercial gain
• You may freely distribute the URL identifying the publication in the public portal

Read more about Creative commons licenses: https://creativecommons.org/licenses/

Take down policy
If you believe that this document breaches copyright please contact us providing details, and we will remove access to the work immediately and investigate your claim.

LUND UNIVERSITY

PO Box 117
221 00 Lund
+46 46-222 00 00

Intensity Dependence of Two-Color Laser-Assisted Photoionization Spectra

M. Swoboda,* J. M. Dahlström, T. Ruchon,† J. Mauritsson, and A. L'Huillier

Division of Atomic Physics, Lund University, P.O. Box 118, 22100 Lund, Sweden

K. J. Schafer

Department of Physics and Astronomy, Louisiana State University, Baton Rouge, Louisiana 70803-4001, USA

(Dated: March 17, 2009)

We study experimentally the influence of the infrared (IR) probing field on attosecond pulse train (APT) phase measurements performed with the RABITT method (Reconstruction of Attosecond Beating by Interference in Two-Photon Transitions). We find that if a strong IR field is applied the attosecond pulses will appear to have lower-than-actual chirp rates. We also observe the onset of the streaking regime in the breakdown of the weak-field RABITT conditions. We present a novel approach to extract the chirp rate of the attosecond emission in the conditions of high IR probe intensities and how to resolve the challenges of the intensity dependence of the RABITT method. We perform a Fourier-analysis of harmonic and sideband continuum states and show that the mutual phase relation of the harmonics can be extracted from higher Fourier components, demonstrating APT characterization methods for all probe intensity regimes.

*Electronic address: `marko.swoboda@fysik.lth.se`; URL: `http://www.atto.fysik.lth.se`

†now at: CEA-Saclay, DSM, Service des Photons, Atomes et Molécules, 91191 Gif sur Yvette, France

I. INTRODUCTION

Laser-assisted ionization processes provide an elegant tool to study dynamics and details of atomic and molecular systems [1–3]. For time-dependent measurements, the assisting laser needs to be synchronous to the ionization event on a time scale below that of the process to be resolved. A number of experiments in the past years have shown that the attosecond (as) time scale is routinely available and laser-assisted ionization processes have become the chief tool for experiments in the field of attosecond science [4, 5].

The emission of a comb of high-order harmonics when an atomic medium is exposed to a driving intense laser field is well understood [6, 7]. The resulting APTs [8, 9] provide a premier tool to controllably ionize atomic media [4, 10] and it is important to know their characteristics, both amplitude and phase. This can be done by cross-correlation with an IR probing field under stable interferometric conditions [11, 12]. Using weak IR fields, this is best done with the RABITT method [8, 13], the case of stronger fields represents the AC-streak camera method [14, 15]. A special case of the latter is the full characterization method FROGCRAB, which is based on an iterative deconvolution of a time-frequency spectrogram [16–18]. In this paper, we study the transition from this single-photon-limit to a multiphoton-limit, its effect on the measured phase and the breakdown of the photon picture.

In the first Section, the experimental setup and performed experiments will be presented. We then perform a conventional analysis of the data in the RABITT and streaking regime, studying specifically the probe intensity dependence of the phase measurement. A Fourier-series-approach then allows us to see the fingerprints of processes with more than one contributing IR photon and provides a more general description of our delay dependent laser-assisted photoionization spectra.

II. EXPERIMENT

A. Setup

The experiments were performed at the High Power Laser Facility of the Lund Laser Centre. We use a 1 kHz chirped-pulse-amplification (CPA) titanium-sapphire based laser system, providing 2 mJ in 30 fs centered around 800 nm. This laser is focused into an Ar gas

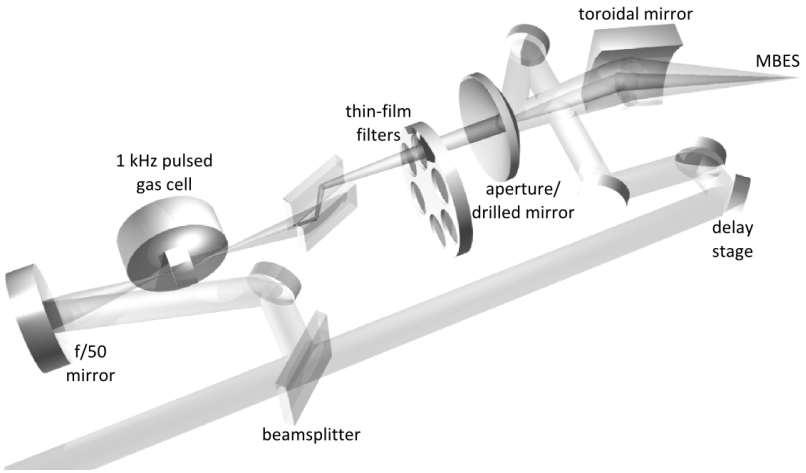

FIG. 1: Setup for the experiment: a 2 mJ, 30 fs laser pulse is split into a probe and a pump arm, the larger part of which is used in high-order harmonic generation, the lesser fraction traveling over a delay stage to serve as delayed probe beam. The generated harmonics are filtered spatially and spectrally by an aperture and a metallic thin-film filter, before recombining with the probe on a drilled mirror and being focused into the detection gas of a magnetic bottle electron spectrometer (MBES).

cell, pulsed at 1 kHz, to generate high-order harmonics, which then propagate through an aperture and a thin Al-foil to filt er the harmonics into a well-defined APT (cf. Fig. 1). The APT is then recombined with an IR probe beam in a Mach-Zehnder-type interferometer comprising a drilled mirror and focused into the detection gas of a magnetic-bottle electron spectrometer (MBES). Using a combination of halfwave plate and polarizer in the probe beam, the pulse energy of the IR can then be varied continuously between 5 and 100 μJ. As all focusing parameters are kept constant, any change in the probe pulse energy will directly result in a proportional change of the IR intensity in the detection region of the MBES. The MBES has a 2π acceptance angle and a maximum energy resolution of about 100 meV.

The relative delay of IR probe and APT can be adjusted on two timescales. Using a motorized translation stage in the probe arm we can vary the delay in the range of one femtosecond to several picoseconds. To accurately resolve attosecond processes, a delay stage with a piezoelectric crystal is used to change the relative phase of the two beams with a precision of several 10 as. This interferometric stability allows us to perform interferometry of two-photon pathways as in the RABITT characterization scheme. It is also crucial to

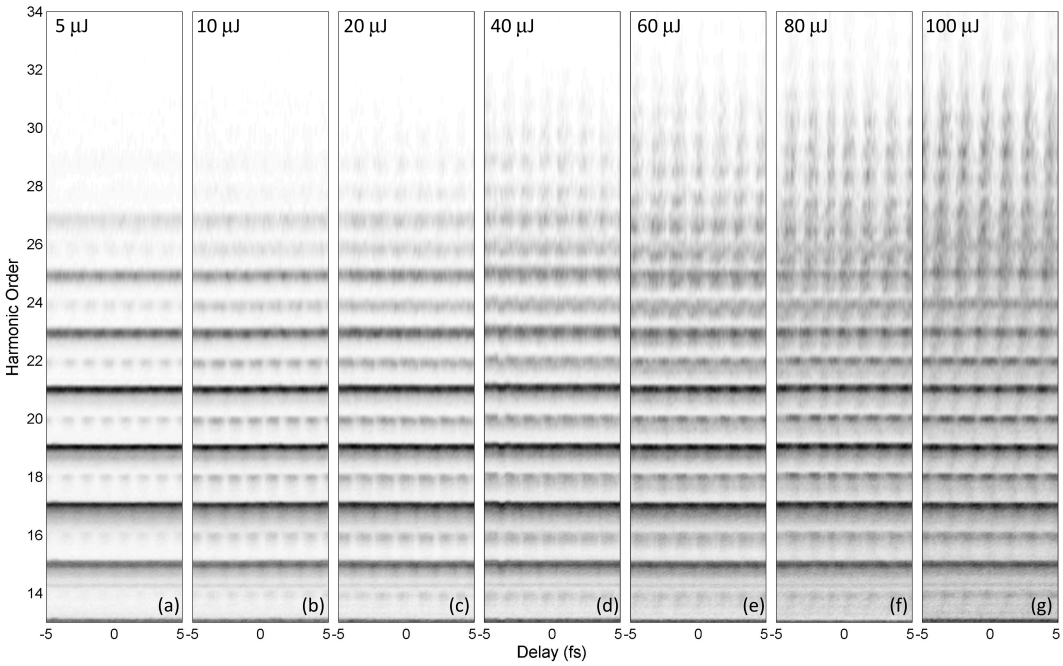

FIG. 2: XUV photoionization spectra, recorded for varying delay between IR and XUV field. The IR intensity is increasing from left to right, with the probe pulse energies written in the upper part of the figure. As focusing and probe pulse diameter were kept constant, a change in the measured pulse energies translates proportionally to a change of the probe intensity. This indicates that the probe pulse energy has changed by a factor of 20 from left to right.

employ the method of the AC streak camera, where the relative phase of the two beams needs to be stable on a similar level.

B. Delay-Dependent Two-Color Photoionization Spectra

In the experiments presented here, the resulting photoelectron spectra from an IR probe and XUV beam were recorded. A shift in the relative delay of both beams will lead to a change of the observed spectrum, and scanning the delay allows us to obtain a time-dependent interferometric measurement of the temporal structure of the XUV emission.

Figure 2 shows the seven scans that constitute the experimental traces for our study. From left to right, the probe pulse energy changes by a factor of 20, ranging from 5 to 100 μJ. For the lowest intensity, the slight perturbation of the photoionization process is visible by the barely visible sidebands between the odd harmonic orders. These sidebands originate

from $\hbar\omega_n + \hbar\omega_R$ and $\hbar\omega_n - \hbar\omega_R$ two-photon transitions [13], with an odd harmonic photon $\omega_n = n\omega_R$ and ω_R the carrier frequency of an IR photon. The possibility of two pathways to each final state leads to the observed interference pattern. This pattern repeats itself every infrared halfcycle $T_R/2$, reproducing the frequency of the attosecond pulse arrival. This probe intensity regime is commonly referred to as the RABITT (Reconstruction of Attosecond Beating by Interference in Two-photon Transitions) regime. Here, the final electron states in the continuum are separated by integer numbers of the initial photon energy, $\hbar\omega_R$.

With increasing IR intensity, the amplitude of the sidebands becomes comparable to that of the odd harmonics (cf. Figure 2d)-g)). The probability for two-photon processes is increased drastically leading to depletion effects in the odd harmonic states populated by single-XUV-photon transitions. Significant population minima in the odd states then occur at the maxima of the sidebands. The cutoff region is first affected by depletion (Fig. 2b) and c)). For a probe pulse energy of 40 μJ (Fig. 2d)), depletion effects become visible in the plateau region between harmonic 19 to 23 (cf. Fig. 2d)-g)).

At these higher probe intensities of Figure 2d)-g), processes involving more than one IR photon begin to occur. This is the so-called streaking regime, where the AC-streak camera method becomes the preferred characterization method, mainly for isolated attosecond pulses [14, 15, 18]. The Streaking method requires relatively high temporal confinement of the attosecond XUV emission.

The streaking regime is clearly entered in the last two of the scans in Fig. 2, at times the cutoff being increased by as much as 7 IR photons. Note that in our case the electron signal is still showing discrete IR photon energy spacing because of the repeated occurrence of photoionization from the sequence of attosecond pulses in our APT.

III. ANALYSIS OF THE EXPERIMENT

A. Reconstruction of Attosecond Beating by Interference in Two-Photon Transitions (RABITT)

To understand the appearance of Figure 3 (same as 2a)), a typical RABITT trace, let us consider the experiment within a perturbation theory framework. Here, we will consider

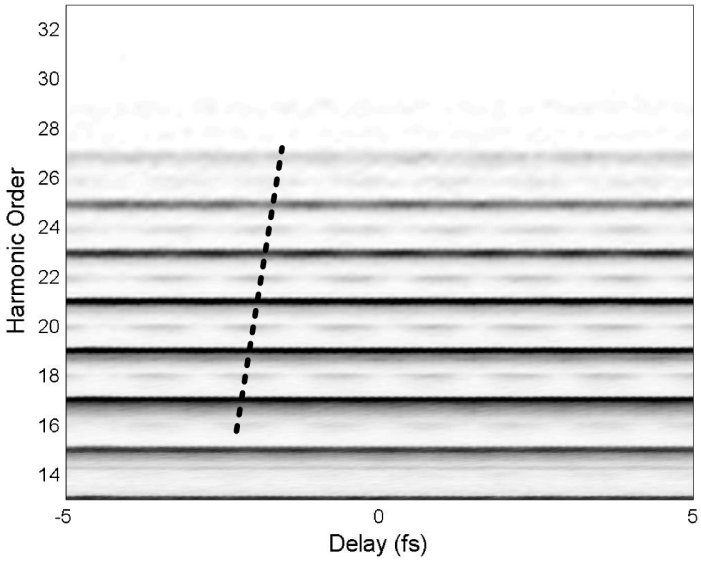

FIG. 3: Delay-dependent photoionization spectrum in the RABITT regime, measured at 5 μJ probe pulse energy. The dashed line indicates the sideband maxima that occur at the probe laser E-field maxima and are used to measure the emission time difference over the spectrum.

the photoionization of the detection gas by the APT as a first-order perturbation and the onset of the sidebands and the RABITT modulation as a perturbation of the second order. This is a good description of two-color photoionization at low IR intensities.

Contributions to the final state probability amplitudes of order N can be obtained from these of order (N-1) through the following equation [19, 20]:

$$a_m^{(N)}(t) = \frac{1}{i\hbar} \sum_f \sum_l \int_0^t dt' \mu_{m,l} E(\omega_f) a_l^{(N-1)}(t') e^{i(\omega_{ml}-\omega_f)t'}, \tag{1}$$

where l is the index of the respective contributing states, ω_f are the frequencies acting on the atom and m denotes the final state. The effect of the IR on the ground state is negligible. Then we find for the population of continuum states after perturbing the system with a harmonic frequency

$$a_n^{(1)}(t) = \frac{\mu_{n,g} E(\omega_n)}{i\hbar} t \tag{2}$$

where $\mu_{n,g}$ is the transition dipole matrix element from the ground to the continuum state, and t the interaction time, approximately a measure of the pulse duration. Figure 4 shows the notation of the levels used from here on. We now look at levels (n) and $(n-2)$ and apply

a second order perturbation with the IR field. For the continuum dynamics we assume the XUV interaction to be negligible, as it contains very few photons compared to the IR. We can then express the population of the sideband state $(n-1)$ as

$$\begin{aligned} a_{n-1}^{(2)}(t) &= \frac{1}{(i\hbar)^2}\frac{t^2}{2}\left[\mu_{n-1,n-2}\mu_{n-2,g}E(\omega_R)E(\omega_{n-2}) + \mu_{n-1,n}\mu_{n,g}E(-\omega_R)E(\omega_n)\right] \\ &\approx M\frac{E_{R0}E_{X0}}{(i\hbar)^2}\frac{t^2}{2}\left[e^{i(\phi_R+\phi_{n-2})} + e^{i(-\phi_R+\phi_n)}\right] \end{aligned} \tag{3}$$

where the factor M represents a combination of the various transition dipole moments, which we approximate as equal for both quantum paths. The harmonic spectral phases ϕ_{n-2} and ϕ_n, will appear as a phase difference $\Delta\phi_{n-2,n}$ contributing to the respective sideband intensity. The sideband intensity will finally oscillate as

$$I_{n-1}^{(2\omega)}(\varphi) \propto \cos\left(2\phi_R + \Delta\phi_{n-2,n}\right), \tag{4}$$

with $\phi_R = \omega_R\tau$ and τ as the delay. This allows us to obtain the phase difference $\Delta\phi_{n-2,n}$ from a Fourier transform of the spectrum over delay.

Using the obtained phase, we can reconstruct a pulse shape as in Figure 5. The Fourier limit for our spectrum is 160 as, yet due to the chirp rate of 18400 as^2 we obtain an average pulse duration of 440 as FWHM. This method of measuring APTs has been successfully employed in a number of experiments [8, 21]. The high chirp rate and asymmetric pulses come as no surprise as no special technique was employed to counter the intrinsic chirp of the HHG process. The addition of more filters would help to approach the Fourier limit and further compress the pulses [21, 22]. As we mentioned earlier, the RABITT method provides access to the relative phase difference of presumably monochromatic harmonics [8, 13]. The obtained phase difference in our experiments equals the group delay (GD) over the spectrum of the APT, and an integration yields the spectral phase and allows the reconstruction of an average attosecond pulse. Such a retrieved pulse represents a good measure of pulses within the FWHM of the APT, accounting for about 90% of the signal from experiments with such trains. There are extensions and implementations of the method that yield more information on the full structure of the APT [12]. They require experimental arrangements differing from ours, however.

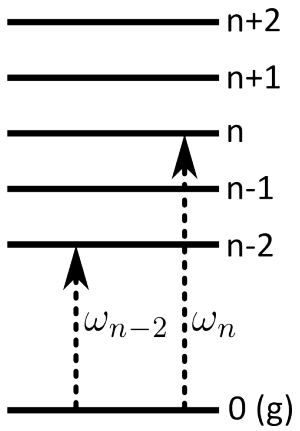

FIG. 4: Notation of continuum levels for perturbation theory. The harmonic levels n,$n-2$ and $n+2$ are odd numbers and can be reached by single harmonic photon absorption.

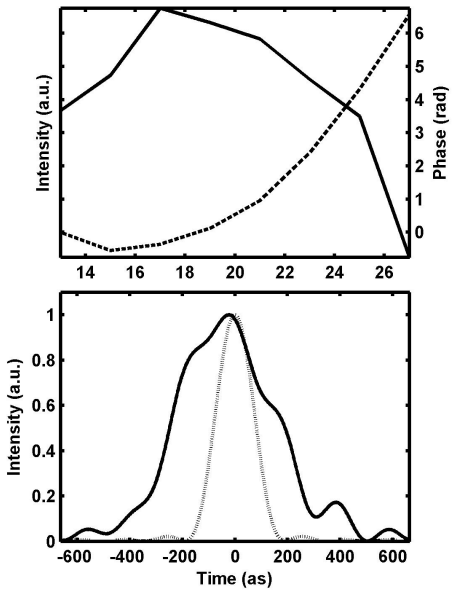

FIG. 5: Reconstruction of average pulse in the pulse train, measured by the RABITT method. The upper panel shows the harmonic intensities (solid line) and integrated spectral phase (dashed line). Using these intensities and phase, one can reconstruct the pulse shape as in the lower panel. The Fourier limited pulse shape is shown as dashed.

B. Intensity Dependence of RABITT Signal

The influence of an ever more intense probe field on the measured spectral phase was studied by progressively increasing the IR intensity and then recording the delay-dependent

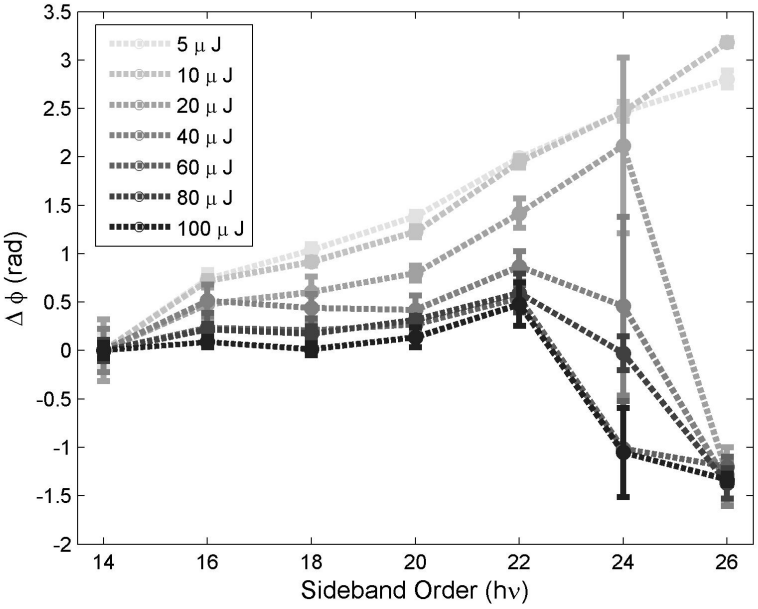

FIG. 6: Phase differences $\Delta\phi$ measured over the harmonic spectrum, dependent on the probe pulse energy. Integrating this function yields the spectral phase ϕ. It is apparent that higher probe intensities result in a flatter measured spectral phase in the plateau region (order 14-22). Sideband order 24 and 26 show a large shift on transition into the streaking regime when the signal is maximized with the maxima of the probe field vector potential.

photoionization spectra. Figure 6 shows the phase differences $\Delta\phi_{n-2,n}$ evolving over the spectrum for varying probe intensity. It is clear that the slope is decreasing with intensity, indicating a lower chirp rate, even though the actual APT remained the same.

Figure 7 shows the influence of the probe pulse intensity on the reconstructed average attosecond pulse structure. A consequence of the phases in Figure 6, the pulses appear more compressed at higher probe intensities. From left to right, the pulse widths measured are 440 as, 380 as and 220 as, respectively. This apparent compression is therefore an artifact of the increased IR intensity.

In RABITT, only the case of a weakly perturbing IR probing field is considered. This means it relies heavily on the presence of a single IR photon contributing to the final state as to allow only the phase difference of the neighboring harmonics to be measured. This is illustrated in Figure 9a), where two harmonics couple in a sideband by a single photon, a second order perturbation. A fourth order process is required to perturb the RABITT signal,

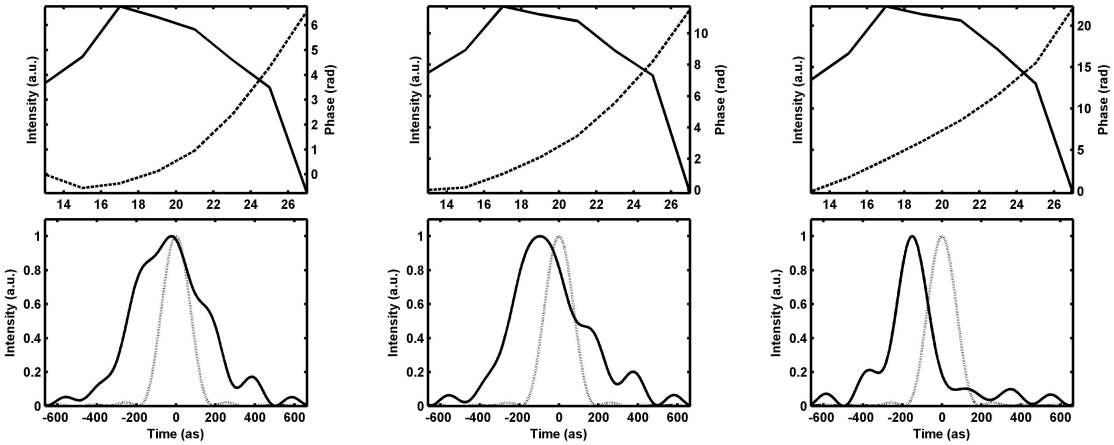

(a)5 μJ (b)10 μJ (c)20 μJ

FIG. 7: Reconstructed average attosecond pulses for probe pulse energies of 5, 10 and 20 μJ. Doubling the IR intensity in going from 5 to 10 μJ shows first compression effects. This even more clear at 20 μJ where the pulses appear to be significantly compressed. This compression, however, is an artifact of too high IR intensities.

as the contribution of two IR photons is acceptable. Neighboring sidebands cannot interact (compare Figure 9) and still only two pathways to the same final state are possible, resulting in an unambiguous interference pattern. We will analyze these multiphoton processes in more detail in Section IV.

C. Streaking

In this subsection, we will study the regime of highest probing intensities, the so-called Streaking[14] regime, where the interaction between photoelectrons and probing laser field can be treated classically. This greatly simplifies the understanding of how the observed delay dependent spectra come about. Figure 8 is a detailed depiction of Figure 2g) and clearly in the Streaking regime, with the cutoff being extended by up to 7 IR photons. Each spectrum of photoelectrons is the result of multiple interferences of electron wave packets with their phase modulated by the IR field[17]. In our case, these wave packets are created every half cycle of the IR field and their carrier envelope phase is shifted by a factor of π.

The attosecond AC streak camera or Streaking method is a tool of primary usefulness for the characterization of single attosecond pulses [14, 15, 18]. In the case of APTs the use of

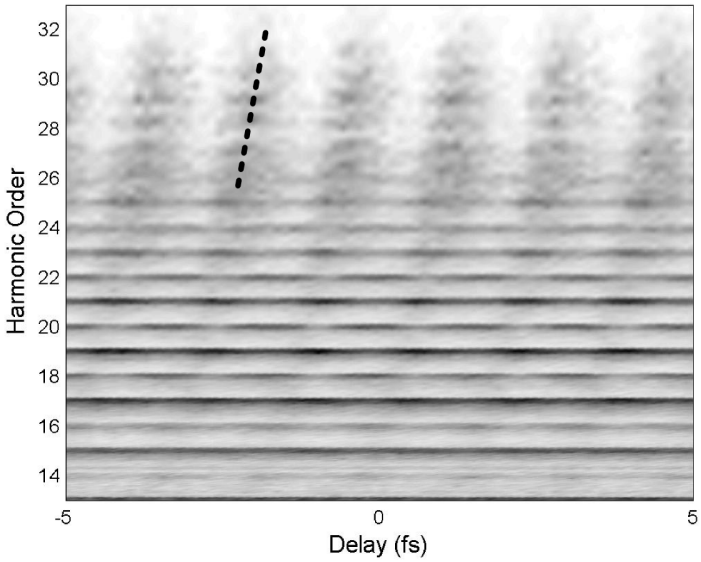

FIG. 8: Delay-dependent photoionization spectrum in the streaking regime, measured at 100 μJ probe pulse energy. The dashed black line illustrates the means of extracting the chirp rate from the cutoff region.

streaking has so far been considered as limited. With two-color generation fields and angular resolution the chirp present from the generation has already been extracted [3, 23].Here, we will show how the cutoff region can be used to extract a meaningful chirp rate.

In Streaking, an electron released into the continuum at a given ionization time t_i due to photoionization will be acted upon by the IR field and will gain momentum proportional the instantaneous IR vector potential $\vec{A}(t_i)$, once both pulses have vanished. This momentum shift imparted by the IR probe is therefore dependent on the relative delay of the two fields. From the simple relation for the kinetic energy $W = \frac{1}{2m}(p_0 + \Delta p)^2 = \frac{1}{2m}(p_0^2 + 2p_0\Delta p + \Delta p^2)$ we see that the energy shift is linear with the instantaneous vector potential ($A \propto \Delta p$) to first order. The largest contribution to the streaking signal originates from the instantaneous frequency for which the vector potential is maximized. In this way we can interpret the slope of the streaking pattern in the cutoff region as dW/dt, the energy slope or chirp rate of the attosecond pulse.

With conventional APTs generated by single-color fields the chirp can be extracted from the cutoff region in scans like Figure 8. Each probe field halfcycle will induce its maximum momentum shift only on one attosecond pulse in the full laser period. As we measure the

kinetic energy of the electrons, the direction of the electrons does not matter. When the attosecond pulse is intrinsically chirped, the maximum streaking effect occurs at different times for different harmonic orders. This can be seen as a tilt in the cutoff region, where the maximum streaking will become dependent on the arrival time of an individual harmonic frequency. This is the distribution of emission times that is extracted as group delay from conventional RABITT measurements. Note that both attosecond pulses that occur during a probe laser period interfere in the plateau region give therefore no meaningful chirp rate, underlining the importance of only considering the cutoff region.

Here, we make use of the fact that we have well-characterized APTs from our previous measurements. This allows us to compare the chirp rates extracted from Streaking to the measurements from RABITT. By fitting a line to the maxima in Figure 8, we obtain a slope of $\Delta t_e = 87\,\mathrm{as}$ or a chirp rate of $18400\,\mathrm{as}^2$, being in extremely good agreement with the RABITT measurement. Comparing this to chirp rates extracted from the two scans of lower probing intensity (Figures 2e) and f)), we find an average $\Delta t_e = 80 \pm 10\,\mathrm{as}$. This is again in very good agreement with the RABITT measurement.

To verify the importance of only considering the cutoff region, we extracted Δt_e in the plateau region of Figure 8 and it amounted to only 21 as, showing the phase flattening already observed in the intensity dependence measurements of the RABITT method. This lining up of the sideband maxima is the consequence of a great number of contributing photons, which will average the phase of the $2\omega_R$ oscillation over the whole spectrum with contributions from almost all harmonics of the spectrum at once.

Finally, the onset of the streaking regime also explains the observed phase shift of the sideband orders close to the cutoff in Figure 6. In the perturbative regime, the maxima of the sidebands occur at the maxima of the probe laser electric field. Stronger depletion of the harmonic states will lead to maxima of the harmonics shifted by π with respect to the sidebands. For the higher probe intensities of Figure 6, the streaking regime is entered and the streaking maxima of plateau harmonics dominate over sideband amplitudes in the cutoff region shifting to the occurrence of the maximum amplitude with the maximum vector potential, i.e. a maximal momentum kick.

IV. FOURIER DECOMPOSITION OF THE PHOTOELECTRON SPECTRA

A. Perturbation Theory Analysis

To better understand the influence of higher IR intensities on the RABITT measurement, we will go back to consider the resulting photoelectron spectra from a two-color photoionization process treated as perturbation.

Looking at the third order of perturbation, we find that this order, which corresponds to a stronger IR field, will contain components coupling the states $(n+2)$ and $(n-2)$ in the harmonic (n) state (cf. Fig.4):

$$\begin{aligned} a_n^{(3)} &= \frac{1}{(i\hbar)^3}\frac{t^3}{6}\left[\mu_{n,n-1}\mu_{n-1,n-2}\mu_{n-2,g}E(\omega_R)E(\omega_R)E(\omega_{n-2}) + \mu_{n,n-1}\mu_{n-1,n}\mu_{n,g}E(\omega_R)E(-\omega_R)E(\omega_n)\right. \\ &+ \left.\mu_{n,n+1}\mu_{n+1,n}\mu_{n,g}E(-\omega_R)E(\omega_R)E(\omega_n) + \mu_{n,n+1}\mu_{n+1,n+2}\mu_{n+2,g}E(-\omega_R)E(-\omega_R)E(\omega_{n+2})\right] \\ &\approx M\frac{E_{R0}^2 E_{X0}}{(i\hbar)^3}\frac{t^3}{6}\left[e^{i(2\phi_R+\phi_{n-2})} + 2e^{i\phi_n} + e^{i(-2\phi_R+\phi_{n+2})}\right] \end{aligned} \tag{5}$$

giving rise to a cosine term of $4\omega_R$ oscillation with delay in the signal of this harmonic on top of a $2\omega_R$ modulation and a constant term (illustrated in Figure 9b)). The intensity of the $4\omega_R$ modulation at harmonic energy n is

$$I_n^{(4\omega)}(\phi_R) \propto \cos\left(4\phi_R + \Delta\phi_{n-2,n+2}\right) \tag{6}$$

which can be identified as similar to Equation 4. Writing the next order of perturbation, one could then see, that a $6\omega_R$ component would arise in the sideband states and then an $8\omega_R$ component in the harmonic states from the next order of perturbation. Higher IR intensities lead to new and unique couplings of states lying further apart and thus the onset of higher modulation frequencies.

Figure 9 illustrates how the number of pathways that lead to a given modulation frequency is unique only under certain restrictions. Even numbers of contributing photons couple two distant harmonics uniquely in harmonic states and odd numbers couple in the sideband states. Therefore, the 4ω frequency is meaningful only in the harmonic final states, as shown in Eq. 5, the occurring phase difference is that of harmonic states $(n-2)$ and $(n+2)$. A Fourier transform that isolates this component will allow access to the spectral phase in the same way as with the conventional RABITT, looking at the $2\omega_R$ modulation in the

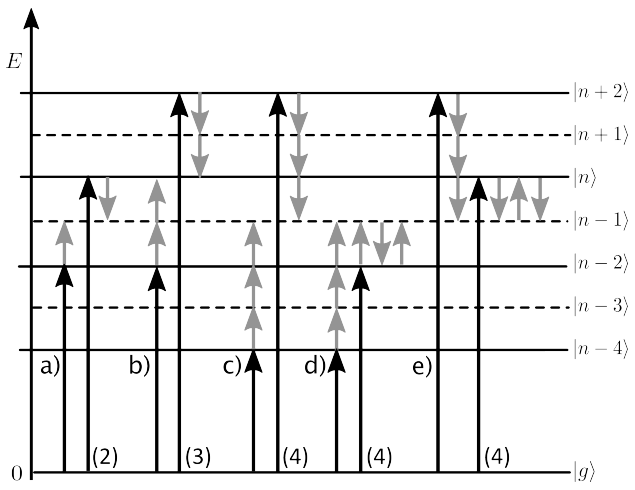

FIG. 9: Sketch over possible multiphoton transitions involving one to three IR photons, a) shows the two-photon transition from ground state to sideband, i.e. common RABITT, which is a second-order perturbation process. b) shows a 3rd perturbation order process, the absorption/emission of two IR photons, yielding a 4ω component in $(2n-1)$. c) shows how a 6ω modulation could be observed in the signal of a sideband, arising from a 4th order perturbation process. d) shows a 4th order process, resulting in a 2ω component, which will perturb the RABITT signal in sideband (2n+1).

sideband states. Experimentally, due to the resolution of our scans, the $6\omega_R$ component is the last resolvable. It is already close to the Nyqvist limit, with only three to four data points per period.

Fig. 10 shows a comparison of the group delay obtained over the spectrum for three different modulation frequencies. The classic RABITT is based on the $5\,\mu$J-scan, the phases of the 4ω-modulation were obtained at $20\,\mu$J, and the 6ω-modulation was present for the central harmonics in the $80\,\mu$J-scan. The reason that the highest IR probing intensity yielded no useful components is probably that then too many different frequency components contribute and thus the overall oscillation contrast is significantly reduced against the noise. One finds, however, excellent agreement between the chirp rates obtained with the different methods. We find also good agreement with previous experiments [9, 21] From the 2ω-measurement we obtain a chirp rate of $18400\,\mathrm{as}^2$ or - in terms of a group delay - an emission time difference $\Delta t_e = \Delta\phi/(2\omega_R) = 87\,\mathrm{as}$. This is very similar to $16800\,\mathrm{as}^2$ ($\Delta t_e = 79\,\mathrm{as}$) obtained from the 4ω-component in the harmonics. The slope of the phase difference in the

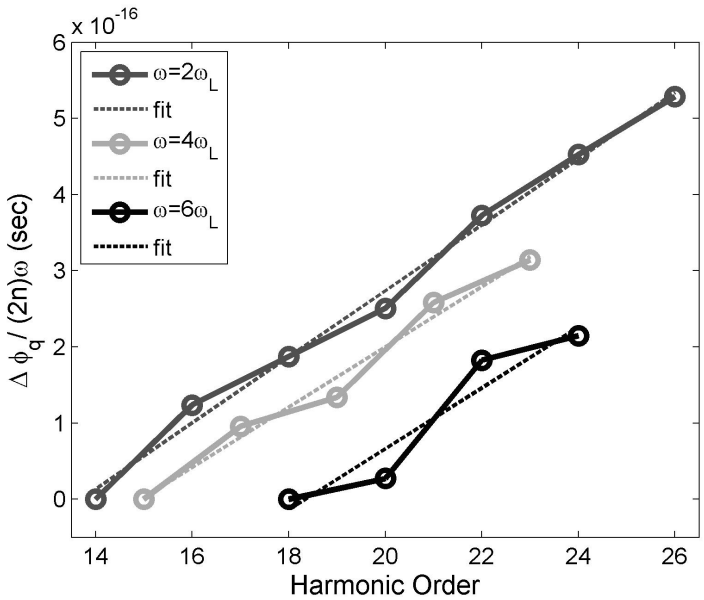

FIG. 10: Comparing the obtained phase differences for 3 different frequency components present in the experimental electron signal. For the conventional RABITT, sidebands from order 14 to 26 contributed. The 4ω-component has been extracted from harmonics 15 to 23 and the 6ω-modulation was obtained from sidebands 18 to 24. The curves have been offset at zero for better comparison.

6ω-component is also in good agreement with 16900 as^2 chirp rate or a Δt_e of 80 as. We note that all three measurements are in good agreement with each other and with the streaking analysis.

B. Generalization

Because of the analogy between the conventional RABITT and the possibility to extract the same information from higher components we will now introduce a more general expression for the delay dependence of our photoelectron spectrum. This expression will hold beyond the breakdown of the perturbation picture. The amplitude of any photoelectron peak in the spectrum is periodic with delay ϕ_R between IR and XUV field. It can therefore be expressed as a discrete Fourier series:

$$S(\phi_R, I_R) = \sum_{n=-\infty}^{\infty} \tilde{S}_n(I_R) e^{i\phi_R 2n} = \sum_{n=1}^{\infty} S_n(\phi_R, I_R) \tag{7}$$

with $\tilde{S}_n^* = \tilde{S}_{-n}$. Considering only the $n = \pm 1$ contributions we have

$$\begin{aligned} S_1(\phi_R, I_R) &= \tilde{S}_1(I_R)e^{i\phi} + \tilde{S}_1^*(I_R)e^{-i\phi} \\ &= 2\,|S_1(I_R)|\cos\Big(2\phi_R + arg(\tilde{S}_1(I_R))\Big) \end{aligned} \tag{8}$$

the common RABITT case, for a low IR intensity, where then $arg(\tilde{S}_1(I_R)) = \Delta\phi_{n-1}$. For higher IR intensities, higher order terms contribute and the argument will change and higher order terms of the sum $\tilde{S}_n(I_R)$ will grow revealing higher contributing frequencies. In the case of $n = 2$

$$\tilde{S}_2(\phi_R, I_R) = 2\,|S_2(I_R)|\cos\Big(4\phi_R + arg(\tilde{S}_2(I_R))\Big)\,. \tag{9}$$

and can readily be identified with the $4\omega_R$ component with an argument of $\Delta\phi_{n-2,n+2}$ for a suitable I_R. Figures 9d)-e) show the effect of the participation of 3 IR photons, and how two non-surrounding harmonics contribute their phase difference to sideband $n-1$, destroying the unique source of the $2\omega_R$ modulation. Thus $arg(\tilde{S}_1(I_R))$ changes, illuminating the IR intensity dependence of the phase in RABITT.

At the same order of perturbation (3 photons, cf. Figure 9d)), a higher harmonic component could be constructed using the participation of 3 IR photons to have a 6ω modulation frequency for the interference pattern in the photoelectron signal in sideband $n-1$, coupling harmonic $n-4$ and $n+2$ by these photons(cf. Fig. 9). For sufficiently high intensity, the number of contributing IR photons is $\gg 1$, resulting in a great number of frequencies added to form the delay-dependent signal in the sideband. Also, all harmonics contribute to the phase and the oscillation does not uniquely depend on the adjacent orders anymore - the requirement for RABITT. This is the streaking regime, where the classical limit is reached.

As we previously studied the effect of the IR intensity on the phase measurement in the conventional RABITT method, we perform a similar analysis for our measurements with the $4\omega_R$ component. Figure 11 shows the intensity dependence of the harmonic phase measured in this component. We find that at 20 to 60 μJ the phase is meaningful compared with the conventional measurement. The measurement at 80 μJ is showing a similar characteristic flattening of the phase as the conventional RABITT. The 4ω breakdown occurs for much higher probe intensities. In this case the number of contributing photons becomes so high that $arg(\tilde{S}_2(I_R))$ is affected by ambiguous coupling of states. Above 80 μJ no useful extraction of phase from the 4ω component is possible due to low oscillation contrast against the background. The analysis of this $4\omega_R$ component provides an additional check on the

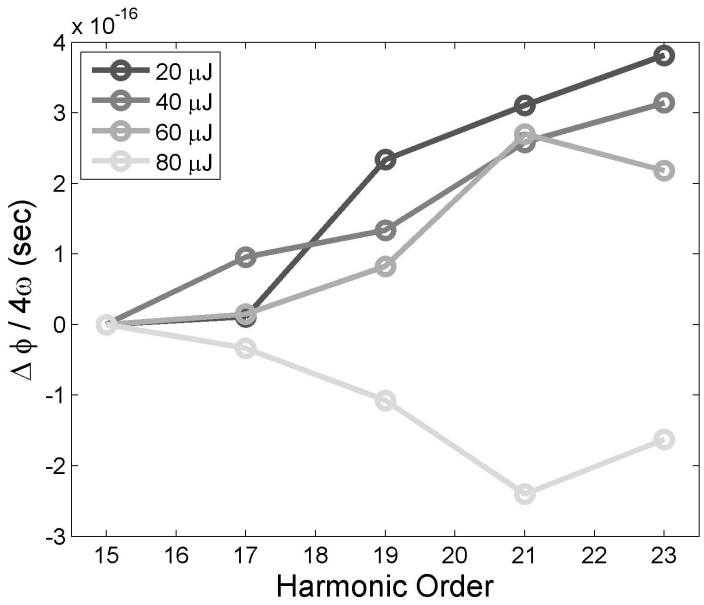

FIG. 11: Intensity dependence of the measured phase from the 4ω component in the harmonics. The measured chirp rate over the spectrum shows good agreement at $40\,\mu$J with the 2ω-measurement from the sidebands. It breaks down at the highest probe energies.

measured phase from conventional RABITT method. This allows us to assess whether the probe intensities in any experiment have been too high by comparing the 2ω with the 4ω components and possibly even higher orders.

V. CONCLUSION

We have studied the influence of IR probe intensity in two-color XUV photoionization experiments. In the laser-assisted ionization process that is at the heart of the RABITT method for characterizing APTs, as expected, it turns out that the probe intensity needs to be maintained at levels which only perturb the process very slightly. Too high a probe intensity will greatly alter the measured phase relation of the individual high-order harmonics, seemingly showing nearly Fourier-limited pulses. One can therefore conclude that RABITT is truly a weak-field-method and in any measurement aimed at obtaining the individual harmonic phases the probing IR intensity is of utmost importance. This has great implications for methods like molecular orbital tomography [24] or other studies of molecular and atomic systems based on RABITT [25, 26] as it presents a great source of errors to the experiments.

In a next step, the increasing number of contributing IR photons was tracked down by Fourier-analysis of sideband and harmonic states. As an increasing number of photons allows to couple states further and further away, higher modulation frequencies occur. The 4ω component of the harmonic states then also allowed to obtain their mutual phase relation. Also in this case the increasing IR intensity started to affect the phase measurement quite early until the pulses appeared artificially compressed. Finally, we showed how the cutoff region in streaked photoelectron spectra from APTs can be used to extract the chirp rate of the harmonic spectrum. This provides a new characterization method for each intensity regime studied in our experiments, stretching from the low-intensity RABITT regime to the high-intensity Streaking regime.

We believe these experiments will allow the scientific community to gain a better understanding of the IR intensity dependence of laser-assisted ionization of a gas using high-order harmonics and to analyze and compare the spectral measurements with new tools.

This research was supported by the Marie Curie Intra-European Fellowship (Attotech), the Marie Curie Research Training Networks (XTRA), the Marie Curie Early Stage Training Site (MAXLAS), the Integrated Initiative of Infrastructure LASERLAB-EUROPE within the 6th European Community Framework Programme, the Knut and Alice Wallenberg Foundation, the Crafoord Foundation, the Swedish Research Council, and the National Science Foundation (Grant No. PHY-0701372).

---

[1] A. L. Cavalieri, N. Mller, T. Uphues, V. S. Yakovlev, A. B. caronka, B. Horvath, B. Schmidt, L. Blmel, R. Holzwarth, S. Hendel, M. Drescher, U. Kleineberg, P. M. Echenique, R. Kienberger, F. Krausz, and U. Heinzmann, Attosecond spectroscopy in condensed matter, Nature **449**, 1029–1032 (2007).

[2] M. Drescher, M. Hentschel, R. Kienberger, M. Uiberacker, V. Yakovlev, A. Scrinzi, T. Westerwalbesloh, U. Kleineberg, U. Heinzmann, and F. Krausz, Time-resolved atomic inner-shell spectroscopy, Nature **419**, 803 (2002).

[3] J. Mauritsson, P. Johnsson, E. Mansten, M. Swoboda, T. Ruchon, A. L'Huillier, and K. J. Schafer, Coherent Electron Scattering Captured by an Attosecond Quantum Stroboscope, Phys. Rev. Lett. **100**, 073003 (2008).

[4] P. Johnsson, J. Mauritsson, T. Remetter, A. L'Huillier, and K. J. Schafer, Attosecond Control of Ionization by Wave-Packet Interference, Phys. Rev. Lett. **99**, 233011 (2007).

[5] T. Remetter, P. Johnsson, J. Mauritsson, K. Varjú, Y. Ni, F. Lépine, E. Gustafsson, M. Kling, J. Khan, R. López-Martens, K. J. Schafer, M. J. J. Vrakking, and A. L'Huillier, Attosecond Electron Wave Packet Interferometry, Nature Phys. **2**, 323 (2006).

[6] M. Lewenstein, P. Salières, and A. L'Huillier, Phase of the atomic polarization in high-order harmonic generation, Phys. Rev. A **52**, 4747 (1995).

[7] M. Lewenstein, P. Balcou, M. Ivanov, A. L'Huillier, and P. B. Corkum, Theory of high-order harmonic generation by low-frequency laser fields, Phys. Rev. A **49**, 2117 (1994).

[8] P. M. Paul, E. S. Toma, P. Breger, G. Mullot, F. Augé, P. Balcou, H. G. Muller, and P. Agostini, Observation of a Train of Attosecond Pulses from High Harmonic Generation, Science **292**, 1689 (2001).

[9] Y. Mairesse, A. de Bohan, L. J. Frasinski, H. Merdji, L. C. Dinu, P. Monchicourt, P. Breger, M. Kovačev, R. Taïeb, B. Carré, H. G. Muller, P. Agostini, and P. Salières, Attosecond Synchronization of High-Harmonic Soft X-rays, Science **302**, 1540 (2003).

[10] O. Guyétand, M. Gisselbrecht, A. Huetz, P. Agostini, R. Taieb, A. Maquet, B. Carre, P. Breger, O. Gobert, D. Garzella, J.-F. Hergott, O. Tcherbakoff, H. Merdji, M. Bougeard, H. Rottke, M. Bottcher, Z. Ansari, and P. Antoine, Evolution of angular distributions in two-colour, few-photon ionization of helium, Journal of Physics B: Atomic, Molecular and Optical Physics **41**(5), 051002 (2008).

[11] P. Johnsson, K. Varjú, T. Remetter, E. Gustafsson, J. Maritsson, R. López-Martens, S. Kazamias, C. Valentin, P. Balcou, M. B. Gaarde, K. J. Schafer, and A. L'Huillier, Trains of attosecond electron wave packets, J. Mod. Opt. **53**, 233 (2006).

[12] K. Varjú, Y. Mairesse, P. Agostini, P. Breger, B. Carré, L. J. Frasinski, E. Gustafsson, P. Johnsson, J. Mauritsson, H. Merdji, P. Monchicourt, A. L'Huillier, and P. Salières, Reconstruction of Attosecond Pulse Trains Using an Adiabatic Phase Expansion, Phys. Rev. Lett. **95**, 243901 (2005).

[13] V. Véniard, R. Taïeb, and A. Maquet, Phase dependence of (N+1) - color (N>1) ir-uv photoionization of atoms with higher harmonics, Phys. Rev. A **54**, 721 (1996).

[14] J. Itatani, F. Quéré, G. L. Yudin, M. Y. Ivanov, F. Krausz, and P. B. Corkum, Attosecond Streak Camera, Phys. Rev. Lett. **88**, 173903 (2002).

[15] E. Goulielmakis, M. Uiberacker, R. Kienberger, A. Baltuska, V. Yakovlev, A. Scrinzi, T. Westerwalbesloh, U. Kleineberg, U. Heinzmann, M. Drescher, and F. Krausz, Direct Measurement of Light Waves, Science **305**, 1267 (2004).

[16] Y. Mairesse and F. Quéré, Frequency-resolved optical gating for complete reconstruction of attosecond bursts, Phys. Rev. A **71**, 011401(R) (2005).

[17] F. Quéré, Y. Mairesse, and J. Itatani, Temporal characterization of attosecond XUV fields, J. Mod. Opt. **52**, 339 (2005).

[18] G. Sansone, E. Benedetti, F. Calegari, C. Vozzi, L. Avaldi, R. Flammini, L. Poletto, P. Villoresi, C. Altucci, R. Velotta, S. Stagira, S. D. Silvestri, and M. Nisoli, Isolated Single-Cycle Attosecond Pulses, Science **314**, 443–446 (2006).

[19] J. J. Sakurai, *Modern Quantum Mechanics*, Addison-Wesley Publishing Co., 1994.

[20] R. W. Boyd, *Nonlinear Optics*, Academic Press, 2003.

[21] R. López-Martens, K. Varjú, P. Johnsson, J. Mauritsson, Y. Mairesse, P. Salières, M. B. Gaarde, K. J. Schafer, A. Persson, S. Svanberg, C.-G. Wahlström, and A. L'Huillier, Amplitude and Phase Control of Attosecond Light Pulses, Phys. Rev. Lett. **94**, 033001 (2005).

[22] K. Varjú, P. Johnsson, R. López-Martens, T. Remetter, E. Gustafsson, J. Mauritsson, M. B. Gaarde, K. J. Schafer, C. Erny, I. Sola, A. Zaïr, E. Constant, E. Cormier, E. Mével, and A. L'Huillier, Experimental Studies of Attosecond Pulse Trains, Laser Physics **15**, 888–898 (2005).

[23] E. Mansten, J. M. Dahlström, P. Johnsson, M. Swoboda, A. L'Huillier, and J. Mauritsson, E. Mansten, J. M. Dahlström, P. Johnsson, M. Swoboda, A. L'Huillier and J. Mauritsson, New. J. Phys. **10 No.8**, 083041 (2008).

[24] J. Itatani, J. Levesque, D. Zeidler, H. Niikura, H. Pépin, J. C. Kieffer, P. B. Corkum, and D. M. Villeneuve, Tomographic imaging of molecular orbitals, Nature **432**, 867 (2004).

[25] S. Haessler, B. Fabre, J. Higuet, J. Caillat, T. Ruchon, P. Breger, B. Carr, E. Constant, A. Maquet, E. Mvel, P. Salires, R. Taib, and Y. Mairesse, Phase-resolved attosecond near-threshold photoionization of molecular nitrogen, Phys. Rev. Lett. , *accepted* (2009).

[26] W. Boutu, S. Haessler, H. Merdji, P. Breger, G. Waters, M. Stankiewicz, L. J. Frasinski, R. Taieb, J. Caillat, A. Maquet, P. Monchicourt, B. Carre, and P. Salieres, Coherent control of attosecond emission from aligned molecules, Nat. Phys. **4**, 545–549 (2008).